Modeling Gold Nanoparticles: Morphology, Electron Structure, and Catalytic Activity in CO Oxidation†

L. Guczi* and D. Horváth

Department of Surface Chemistry and Catalysis, Institute of Isotope and Surface Chemistry, CRC, HAS, P.O. Box 77, H-1525 Budapest, Hungary

Z. Pászti, L. Tóth, Z. E. Horváth, A. Karacs, and G. Petõ

Institute of Technical Physics and Materials Science, P.O. Box 49, H-1525 Budapest, Hungary

Received: July 29, 1999; In Final Form: January 4, 2000

Morphology, electron structure, and catalytic activity in CO oxidation over a $Au/FeO_x/SiO_2/Si(100)$ model sample prepared by pulsed laser deposition (PLD) have been investigated by X-ray photoelectron spectroscopy (XPS), UV photoelectron spectroscopy (UPS), and transmission electron microscopy (TEM). Two types of sample were prepared denoted by PLD I and PLD II, the latter being prepared by multiple laser deposition alternatively by iron and gold. PLD I was characterized in "as prepared" oxidized and reduced states, the respective gold particle sizes being 3.8, 4.1, and 5 nm; the iron oxide support was amorphous after the first two treatments while it was partially crystallized after reduction. The activity in CO oxidation increased after oxidation of the sample, whereas it was diminished after subsequent reduction. XPS studies showed that higher activity was associated with amorphous iron oxide with Fe 2p binding energy = 711.3 eV. It was established that in developing the catalytic activity the gold should be metallic and the support should be amorphous with high binding energy and the reaction occurs at the perimeter of gold particles. PLD II has a slightly lower activity which might be the result of more crystalline phase in the iron oxide.

1. Introduction

Gold is known as one of the most stable noble metals among group 8 elements which are resistant to oxidation and other aggressive environments. This is why the discovery of gold being a very active catalyst when highly dispersed made a great impact on the scientific community. Gold has been used as second component in the platinum-based alloys, the gold being considered as nonmiscible with platinum and segregated to the platinum surface.[1,2]

Although Turkevich produced gold films of uniform size as early as 1972[3] and Galvagno and Parravano investigated the activity of gold in oxygen/hydrogen transfer reactions[4−6] as well as in the NO reduction reaction by hydrogen,[7] gold was known as one of the least reactive noble metals.[8] Its inactivity was attributed to the completely filled 5d shell and the relatively high values of its first ionization potential (9.22 eV).

It is interesting to mention the rank reactivity of the elements suggested by Puddephatt.[9] In the beginning of the 1970s the elements with low binding energies were considered as the most reactive materials (except the noble gases). On that ranking scale, bulk gold possesses one of the lowest cohesion potentials (Cu ∼ Au < Pt) among the transition elements, so according to the above principles gold should have been very reactive.

The research on gold has widened in the years of 1990s and today we know that under certain conditions it is considered as an appropriate metal for catalytic reactions. Haruta et al. discovered that gold nanoparticles supported on Co_3O_4, Fe_2O_3, and TiO_2 oxides have exceptionally high activity for CO and H_2 oxidation,[10,11] NO reduction,[12] water-gas shift reaction,[13] CO_2 hydrogenation,[14] and catalytic combustion of methanol,[15] when dispersion of the gold particles approached 100%.

Since the discovery of the high catalytic activity of gold nanoparticles, several studies have been performed to elucidate the mechanism of the catalytic properties of gold. The still widening research is mainly concerned with the particle size effect, and/or the metal/support interaction. Iwasawa et al. prepared highly dispersed gold clusters by impregnating various metal hydroxides with a solution of $[Au_9(PPh_3)_8](NO_3)_3$ solution and they found that after decomposition the gold clusters deposited on Mn, Fe, Co, Ni, Cu, and Zn hydroxide were active in the CO oxidation even at subambient temperatures.[16] More detailed studies on the $Au/Fe(OH)_3$ system revealed that after calcination the catalyst showed extremely high activity.[17] This was ascribed to the stabilization of $[Au(PPh_3)]^+$ species leading to small gold particles. On the other hand, when the complex deposited on Fe_2O_3 was decomposed, large gold particles were formed with very low activity in CO oxidation. On the contrary, other authors suggested that the catalytic activity can be assigned to the presence of ferrihydrate activating molecular oxygen.[18] They also observed Au^0 and Au^{3+} species, but no direct correlation was found between the valence state of gold and the catalytic activity. In the later work they identified Au^+ species being more active than Au^0 particles.[19] The importance of metal hydroxide as support seems to be supported by the high activity of $Au/Ni(OH)_2$ in the water-gas shift reaction.[20]

Stabilization of small gold particles was achieved by inserting gold into zeolite supercages.[21−24] When gold in the form of $[Au(en)_2]^{3+}$ complex is located in NaHY, gold particles whose size

* Corresponding author. Fax: +361-395-9001. E-mail: guczi@alpha0.iki.kfki.hu.

† Part of the special issue "Gabor Somorjai Festschrift".

10.1021/jp992662k CCC: $19.00
Published on Web 02/16/2000

depends on the number of protons being in the cation exchange position (smaller number of protons results in smaller gold particle size) are formed by autoreduction.[22] ^{129}Xe and DRIFT studies indicated the presence of $Au^{\delta+}$ species;[23] this, however, could be the result of CO chemisorption.[25] Nevertheless, bimetallic PdAu particles can also be produced by this method.[21] Ichikawa prepared Au/NaY and Au(I)/NaY samples and they observed higher activity due to the presence of the latter species. This points to the mixing effect of the positively charged and zerovalent gold particles.

The literature thus suggests that the main factor in preparing active gold catalysts is that the support must be a redox system (TiO_2, MnO_2, Fe_2O_3, Co_3O_4, etc.). However, in a recent paper[26] gold was deposited on $Mg(OH)_2$ and it was shown by structural studies that below 1 nm size the gold particles exist in icosahedral symmetry whereas above 1 nm the gold is in fcc cuboctahedral symmetry. This indicates that the geometrical symmetry is also an important factor in developing high activity.

In spite of the catalytic results there is still no direct evidence available on how gold nanoparticles become active in the catalytic reactions. What we know is that gold species must be in the nanosize diameter range on the supports. It is difficult to deposit gold on metal oxides with dispersion as high as, e.g., for platinum which has a higher melting point (1769 °C). Gold is very sensitive to preparation methods, pretreatments and the supports used. The use of coprecipitation and deposition−precipitation methods can produce such small gold particles which have high catalytic activity. Other novel methods of preparation include arc melting, chemical vapor deposition, cosputtering,[27] and pulsed laser deposition (PLD).[28]

In this work, our aim is to prepare model Au catalysts on a well-defined Si(100) surface and to find a correlation between the electronic properties and the catalytic activity. The model catalysts were prepared by the pulsed laser deposition (PLD) technique in which thin, islandlike layers of Au were deposited on Si(100) and FeO_x/SiO_x/Si(100) surfaces. We chose iron oxide as support because it can change its oxidation state easily and thus could cause an alteration in the electronic structure of gold particles. All changes in the structure and electronic properties of the catalysts are correlated to the catalytic activities of the samples. The structure and the electronic properties are investigated by transmission electron microscopy (TEM), UV photoelectron spectroscopy (UPS), and X-ray photoelectron spectroscopy (XPS). CO oxidation was chosen as the test reaction with products analyzed by mass spectrometry. Thereby it is hoped that some composition/structure−activity relationship can be established in order to explain the increase in the activity of gold.

2. Experimental Section

2.1. Sample Preparation. The Au containing iron oxide model catalysts were prepared by pulsed laser deposition (PLD),[28] with appropriate control of the amount of deposited material. The catalysts were prepared by using the fundamental wavelength output (1064 nm) of a pulsed Q-switched Nd:glass laser with 35 ns pulse width and 1 Hz repetition rate. The laser beam was focused into a spot of 2 mm^2, which resulted in a laser flux of about 10 J/cm^2 on the target surface. The deposition process was carried out in a small ion-pumped vacuum system with base pressure around 1×10^{-7} mbar. The film thickness was monitored during deposition by a quartz crystal oscillator microbalance.

The 100 nm thick SiO_2 covered Si(100) wafer substrates were introduced into the vacuum system after degreasing in acetone. Substrates were always kept at room temperature. The target−substrate distance was set to 7 cm, and the target normal intersected the center of the substrate, while the angle of incidence of the laser beam onto the target was around 30° with respect to its normal.

In previous studies on nanoparticle nucleation during pulsed laser deposition,[29] it was demonstrated that, if the particle formation takes place on the surface of a support material, the resulting particle shape is oblate ellipsoid; i.e., rather flat, nearly two-dimensional islands are formed. On the other hand, if the deposition is carried out in the presence of a background gas, vapor phase homogeneous particle nucleation can be achieved[30] with more or less spherical particle shapes. Thus, in order to investigate the effect of the particle geometry on the catalytic properties, two kinds of samples were prepared. On the first type, gold islands are grown on the top of an iron oxide layer (from now on denoted as PLD I), while in the second case the catalyst contains spherical gold particles embedded in an iron oxide matrix with the aim of producing a better gold dispersion (denoted as PLD II).

For preparation of the PLD I sample, 10 nm iron oxide was directly deposited onto the SiO_2 surface in 0.2 mbar of O_2; then the chamber was pumped down again to 1×10^{-6} mbar, followed by evaporation of 1 nm Au in a vacuum onto the top of the FeO_x layer. In this experiment, an amorphous carbon covered transmission electron microscope microgrid was also used as substrate.

For deposition of the PLD II sample a 40 nm thick iron reference layer was first grown onto the SiO_2 surface in a vacuum. Then O_2 gas was introduced into the camber to ensure the formation of iron oxide with a pressure maintained at 0.2 mbar during film growth. The Au-containing FeO_x layer was deposited by cycles of alternate ablation of the Fe and the Au target (20 pulses to the Fe target and five shots to the Au, repeated until the required thickness is reached) in the above-described atmosphere. The total thickness of the PLD II film was set to 260 nm.

2.2. Sample Characterization. *2.2.1. XPS and UPS Investigations*. Composition and chemical states of the constituents as well as electronic structure of the catalysts were investigated by photoelectron spectroscopy in a Kratos ES-300 type electron spectrometer. For chemical analysis core levels were excited by Al Kα radiation, while valence band spectra were recorded using both UV (He I and II) and X-ray (Al Kα) radiation. The spectra were taken by the FRR mode, and the Cu sample holder was used as binding energy reference.

FeO_x/SiO_2/Si(100) and both Au/FeO_x/SiO_2/Si(100) samples (PLD I and PLD II) samples were characterized by photoelectron spectroscopy in the as-prepared state after Ar^+ ion sputtering for various times. The surface composition was also determined in the samples used in CO oxidation. In several cases the samples were cleaned or depth profiled with 2 keV Ar^+ ion bombardment at a flux of $(1-2) \times 10^{13}$ ion/(cm^2 s). The thermal stability of the PLD I sample was analyzed in a separate experiment by subsequent in situ heat treatments up to 600 °C.

The core level spectra were evaluated by Shirley background subtraction followed by fitting with Gaussian−Lorentzian product peaks.

The change in the valence state of gold and iron oxide in the samples after oxidation and reduction was studied in situ in a reaction cell attached to a KRATOS XSAM 800 XPS machine. Spectra were taken on the as-prepared, oxidized, and reduced samples. The same pretreatment was applied before catalytic measurements. For this analysis we used the Al Kα radiation,

the FAT operating mode, and the carbon peaks as reference. The results obtained by the two different methods on the same samples agreed very well.

2.2.2. Transmission Electron Spectroscopy. Microstructure and morphology of the samples before and after the catalytic runs were determined by transmission electron microscopy (TEM) using a Philips CM-20 type microscope.

A piece from the PLD II sample was ion milled for cross-sectional analysis, while the lateral morphology of the PLD I sample was investigated by plan-view imaging the layer deposited onto the microgrid prepared simultaneously with the silicon-supported catalyst. The sample was pretreated using the same conditions as used for the samples conditions used for XPS and catalytic measurements.

2.3. Catalytic Measurements. CO oxidation by dioxygen was applied as catalytic test reaction. This reaction has a well-known mechanism on several supported metal surfaces like Pt[31] and Pd,[32] and in recent years several CO experiments using supported gold catalysts[33−35] have been reported.

The test reactions were carried out in an all-glass circulation reactor linked to a mass spectrometer via capillary leak. The change in the CO and CO_2 concentration with time was followed using the same gas composition and the same total pressure in the reactor. The amount of CO_2 was measured at a standard 180 mbar pressure controlling the $m/e = 44$ peak intensity. The initial gas mixture in every case was 10 mbar of CO + 10 mbar of O_2 + 180 mbar of He, resulting in 200 mbar total pressure. He was used as an inert standard. This composition of the reactant gases was chosen after our preliminary experiments revealed it to be the most effective. The investigations were performed on the as-prepared, oxidized, and reduced ones. The oxidized catalysts were pretreated in 150 mbar of O_2 at 200 °C for 1 h, and the reduced ones were reduced in 150 mbar of hydrogen at 200 °C for 1 h. The reactions were performed at 250 °C. The high reaction temperature was necessitated by the low surface area of the samples. Because of the preparation method (PLD) the area of the silica support was limited and was about 0.5−1 cm^2. Moreover, only one side of the support is covered by catalyst material. On these low surface area samples there are only a few active sites for the reaction; therefore, we had to choose the reaction conditions very carefully and we had to employ this high temperature to have an easily detectable amount of reaction product. Because at this temperature the supports could have their own catalytic activity toward CO oxidation, the pure supports were also investigated at the same conditions as the gold-containing samples.

For calculating the amount of CO_2 formed with reaction time, a preliminary calibration of the equipment was performed. The amount of CO_2 was evaluated on the basis of the calibration equation and the measured intensity of the peak $m/e = 44$ after correction with the background. In the background spectra of the MS there was always detectable CO_2 because the spectrometer filament catalyzed CO + O_2 reaction to a certain degree. The amount of CO_2 in the background was always determined by separate measurements.

3. Results and Discussion

3.1. Preliminary Investigations. Preliminary investigations were carried out to create a simple, well-defined model catalyst containing gold as active material which can be well characterized. An islandlike Au film was deposited by pulsed laser deposition onto a Si(100) substrate covered by native oxide. In order to investigate the effect of gold particle size on the electronic structure, the sample was sputtered by 2 keV energy

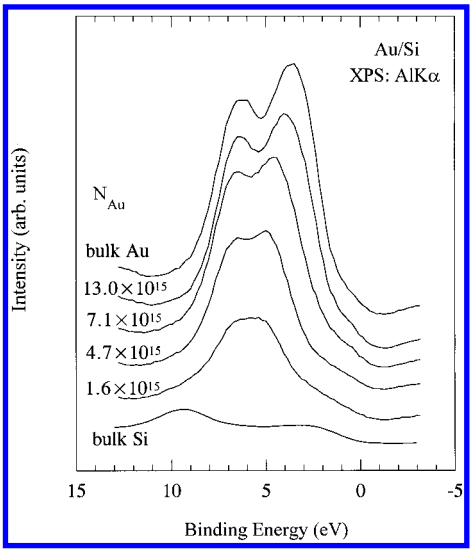

Figure 1. Valence band XPS spectra of islandlike gold film deposited onto silicon at different stages of the sputtering process. N_{Au} indicates the surface concentration of gold.

Ar^+ ions, while XPS spectra were recorded at different stages of the sputtering process (Figure 1). As the sputtering proceeded, the position of the 5d valence band started shifting toward higher binding energy values indicating a transition from bulk to atomically dispersed gold on silicon, while retaining their metallic character. There was no increase in the catalytic activity compared to the pure SiO_x/Si(100) support. This fact suggests that not only the particle diameter and the related changes in the electronic structure are important for the gold to become an active catalyst, at least not in this range of particle size. Indeed, Haruta et al. already showed the effect of particle size in the case of nonredox support, like $Mg(OH)_2$, but gold particles were in a much smaller size range (about 1 nm).[26]

In order to study the effect of support, we prepared an iron oxide containing silicon support, FeO_x/SiO_x/Si(100), and its gold-containing counterpart, a $Au/FeO_x/SiO_x$/Si(100) sample. We used the PLD I preparation technique, and the gold content was the same as in the Au/SiO_x/Si(100) sample. Ion-bombardment-induced size reduction caused significantly smaller changes in the valence band spectra of the sample compared to the Au/SiO_x/Si(100) system. Only the lower binding energy component of the Au 5d peak was slightly shifted toward the higher BE values, which indicated certain rearrangement in the gold 5d states (Figure 2.). This was accompanied by a slight shift of the Au 4f core levels toward higher binding energies. On the other hand, there were remarkable increases in the catalytic activity measured at 250 °C which were 0.9×10^{-3}, 1×10^{-3}, 2.2×10^{-3}, and 3.4×10^{-3} μmol mg^{-1} min^{-1} for SiO_x/Si(100), Au/SiO_x/Si(100), FeO_x/SiO_x/Si(100) and Au/FeO/SiO/Si(100), respectively.

3.2. Effect of Pretreatments on Gold Nanoparticles. We established that among the samples investigated the $Au/FeO_x/SiO_x$/Si(100) samples proved to be the most active catalyst in CO oxidation. In order to study the effect of pretreatments, further experiments were performed on the samples prepared by PLD I and PLD II techniques.

3.2.1. XPS and TEM Measurements on the As-Prepared Samples. Since the samples were prepared by ex situ PLD it is expected that their surfaces are covered by a hydrocarbon- and water-containing overlayer. Thus, before any attempts to evaluate the core level intensity data, overlayer correction had to be employed. For the analysis of the PLD II samples, we used the

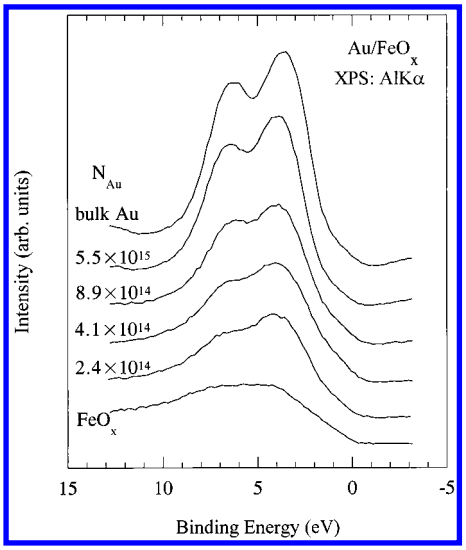

Figure 2. Valence band XPS spectra of island like gold film deposited onto FeO_x at different stages of the sputtering process. N_{Au} indicates the surface concentration of gold.

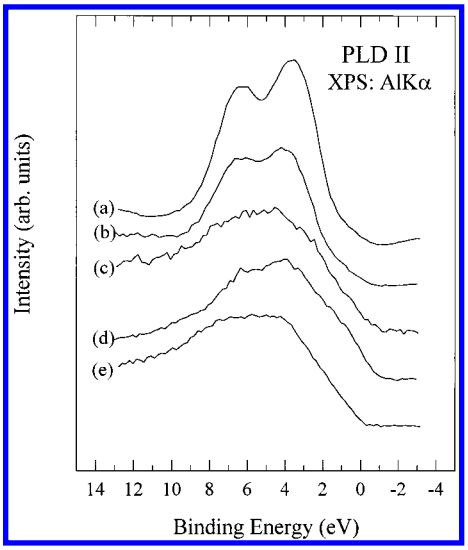

Figure 3. Valence band spectra of PLD II sample: (a) bulk Au; (b) Au in FeO_x as prepared; (c) Au in FeO_x after catalytic measurement; (d) Au in FeO_x after catalytic measurement and extended ion bombardment; (e) FeO_x reference.

TABLE 1: Composition and Core Level Characteristics of the FeO_x Substrate

treatment	composition (atom %)	binding energy (eV)	possible chemical state
2 min 2 keV	[Fe] 39.3	Fe($2p_{3/2}$) 710.6	$Fe^{3+} + Fe^{2+}$
Ar^+ ion	[O] 45.8	O(1s) 530.1	Fe−O
bombardment		O(1s) 531.5	−OH
	[C] 14.8	C(1s) 285.1	hydrocarbons
10 min 2 keV	[Fe] 44.3	Fe($2p_{3/2}$) 710.6	$Fe^{3+} + Fe^{2+}$
Ar^+ ion	[O] 49.8	O(1s) 530.2	Fe−O
bombardment		O(1s) 531.6	−OH
	[C] 5.9	C(1s) 285.1	hydrocarbons

method described by Zalm;[36] however, in the case of the PLD I system a different approach was required.

In Tables 1 and 2 the Au 4f and Fe 2p core level data characteristic of $Au/FeO_x/SiO_x/Si(100)$ samples prepared by PLD I and of PLD II, respectively, in the as-prepared state are presented. In Table 1 the data show that carbon can efficiently be removed by Ar^+ ion bombardment which proves that it is indeed present on the surface region. The surface composition of iron oxide is approximately $Fe_{0.46}O_{0.54}$ and lies between stoichiometric composition of FeO and Fe_3O_4, indicating the presence of Fe^{3+} and Fe^{2+} ions. This is in good agreement with the binding energy of the Fe $2p_{3/2}$ peak. Further Ar^+ ion bombardment only slightly alters the composition. The lack of local charging effects is reflected in the binding energy of the C 1s peak, which coincides with the value suggested for hydrocarbons in the literature. The peak shape can be fitted with a single Gaussian−Lorentzian approach. Fitting the O 1s peak, however, always requires at least two components, the larger one appearing at about 530.0 eV, which is characteristic of Fe−O bonds. The smaller component lies at about 531.7 eV, indicating the presence of O−H bonds even after extended ion bombardment. Moreover, a third component must also be assumed to obtain satisfactory fits, especially for the nonsputtered samples. This peak, located at about 533.0 eV, originates from the water adsorbed in the contamination layer.

In Table 2, XPS the data concerning PLD II sample in the as-prepared state are presented. Since the carbon content is relatively high, an overlayer correction algorithm was applied, giving an overlayer thickness of about 0.4 nm. The properties of the FeO_x matrix are similar to those prepared without gold. The gold content of the sample was determined by assuming that gold was dispersed at atomic level. This simplification may lead to underestimation of the real gold content, when gold is condensed into particles with sizes comparable to the mean free path of the photoelectrons ejected from the Au 4f levels of Au matrix. Binding energy of the Au $4f_{7/2}$ peak is somewhat larger than that in the bulk.

Close inspection of the gold valence band spectra (see Figure 3) revealed some changes. First of all, there was a small shift in the lower binding energy component of the Au 5d states, similarly to what was observed during sputtering-induced size reduction of Au islands on FeO_x (Figure 2). These findings suggest that a part of the Au content may be present in the

TABLE 2: Composition and Core Level Characteristics of As-Prepared PLD II Sample

treatment	composition (atom %)[a] as measured	composition (atom %)[a] corrected[b]	binding energy (eV)	chemical state	Au density (atoms/cm³)
as prepared	[Au] 5.7	[Au] 6.6	Au($4f_{7/2}$) 84.3		
	[Fe] 34.6	[Fe] 45.4	Fe($2p_{3/2}$) 710.8	$Fe^{3+} + Fe^{2+}$	
	[O] 38.5	[O] 47.9	O(1s) 530.2	Fe−O	
			O(1s) 532.0	−OH	
	[C] 21.2	$D_C \approx 0.4$ nm	C(1s) 284.9	hydrocarbons	
5 min 2 keV	[Au] 6.1		Au($4f_{7/2}$) 84.3		
Ar^+ ion	[Fe] 37.8		Fe($2p_{3/2}$) 710.6	$Fe^{3+} + Fe^{2+}$	
bombardment	[O] 42.8		O(1s) 530.0	Fe−O	$(7 \pm 1.5) \times 10^{21}$
			O(1s) 531.5	−OH	
	[C] 13.3		C(1s) 285.0	hydrocarbons	

[a] Determined as if Au would be homogeneously dispersed throughout the FeO_x matrix. [b] Corrected for a carbon- and oxygen-containing overlayer as described in ref. 36.

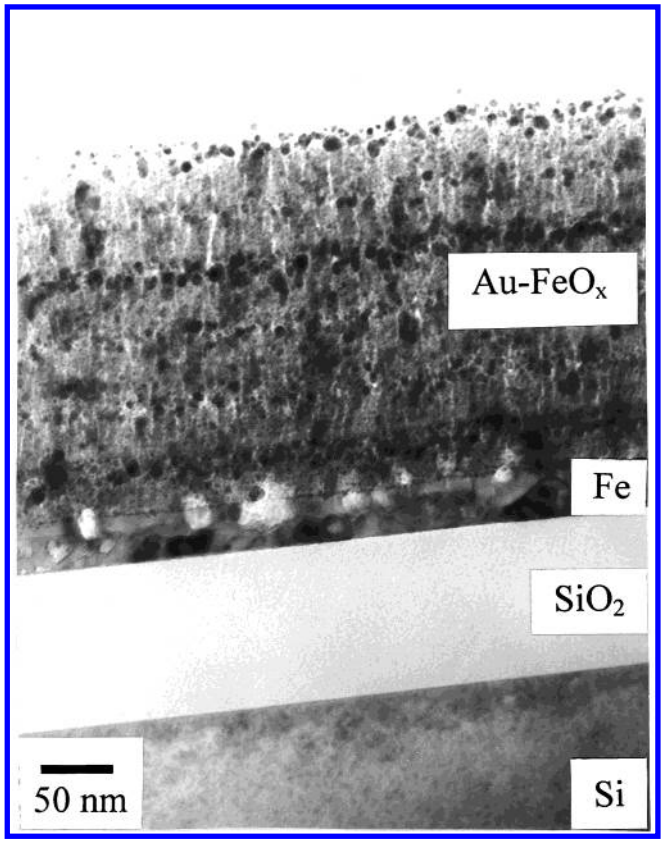

Figure 4. Cross-sectional TEM micrograph of the as-prepared PLD II sample.

form of extremely small particles or even in atomically dispersed state throughout the FeO_x matrix, which is in fact a natural consequence of the nonequilibrium preparation process and is in good agreement with the TEM results.

The microstructure of the PLD II sample was investigated by cross-sectional TEM. A typical micrograph is given in Figure 4. where the overall structure as well as the microstructure of the PLD II layer is easily observable. The Si(100) substrate is covered by a 100 nm thick thermally grown amorphous SiO_2 layer. A 40 nm thick polycrystalline Fe film is grown onto SiO_2, which is covered by the 260 nm thick Au/FeO_x species. In the FeO_x matrix, 3−4 dark strips consisting of relatively large and more or less spherical particles, are visible. Considering the much stronger contrast of these particles compared to even the pure Fe layer, they can be identified as gold precipitates (i.e., gold is a much stronger scattering material for the incoming electron beam, due to its higher atomic number). However, when the deposition parameters were chosen to give homogeneous Au/FeO_x mixture at a significantly finer level, i.e., monolayer amounts were successively ablated from both targets, these strips of particles did not represent the total Au content. Indeed, between the strips a large number of very small particles is visible. Thus, the strips may have been formed by coalescence of these small Au particles, possibly at the actual surface, when the deposition was stopped for a while. The presence of such a strip at the surface at the end of preparation of the sample supports this assumption. The resulting size distribution taken in the vicinity of the surface is, therefore, completely asymmetric as shown in Figure 5.

In addition, the FeO_x matrix has an amorphous structure. This microstructure is due to the room temperature deposition, as opposed to pulsed laser deposition at elevated temperatures, which results in the formation of crystalline iron oxides.[37,38]

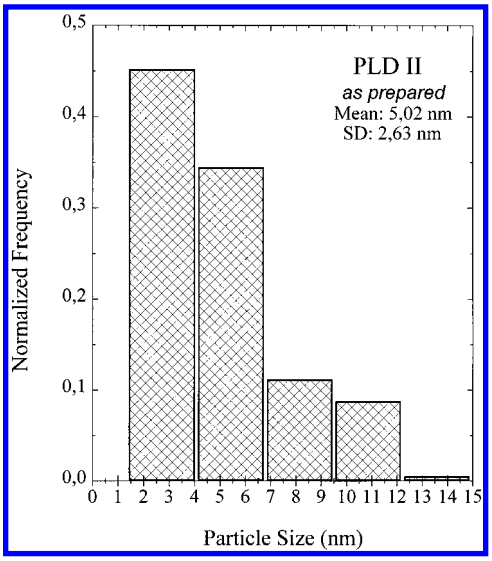

Figure 5. Size distribution of the gold particles in the as-prepared PLD II sample.

The electron diffraction pattern is dominated by the signals resulting from different iron oxide phases as well as from metallic gold. Since the lattice spacing of the different FeO_x phases are close to each other and also close to gold, the phase identification based on diffraction data is impossible.

For PLD I prepared sample the evaluation of the XPS intensity data was somewhat more complicated than in the case of the PLD II sample. The as-measured intensity data as well as the attempts for cleaning the sample by ion bombardment clearly proved the presence of a contaminating overlayer. However, direct application of the overlayer correction algorithm gave unacceptably high amounts of Au with an overlayer thickness of about 2 nm. In addition, the UPS spectra clearly show that gold is present only in a few tenths of nanometers thickness (i.e., comparable to the mean free path of UV excited electrons through the overlayer). Thus, the intensity values were evaluated using a model which assumed that a certain part (determined from TEM images) of the FeO_x support is covered by clean gold islands, while the remaining part is located under a carbon- and water-containing layer. This model, although still oversimplified, fits the measured intensities quite well and gives physically reasonable gold contents and support compositions.

Composition and core level characteristics of the freshly prepared PLD I sample are shown in the first row of Table 3. The thickness of the Au islands calculated from the mentioned model is around 2 nm, which is again a reasonable value and corresponds to the expectation of formation of oblate-shaped ellipsoidal islands.

In a separate experiment we intended to examine the thermal stability of the PLD I sample. The electronic structure and composition were investigated by XPS after 30 min annealing in a vacuum by increasing temperatures a stepwise manner from room temperature to 600 °C. The data are summarized in Table 3 and the valence band spectra are presented in Figure 6. Up to 300 °C the substrate composition determined according to the model described above is close to that of Fe_2O_3, in line with the Fe $2p_{3/2}$ binding energy. In the valence band spectra the structures related to the Au 5d and Au 6s bands are clearly distinguishable from the contribution resulting from the support and are practically the same as in bulk Au indicated by the Au $4f_{7/2}$ binding energy being equivalent to the bulk value. At higher temperatures the reduction of the iron oxide is apparent, and above 500 °C even pure metallic iron becomes detectable, which

TABLE 3: Composition and Core Level Characteristics of PLD I Sample

heat treatment	composition (atom %) as measured[a]	composition (atom %) corrected[b]	binding energy (eV)	chemical state	Au surface concn (atoms/cm^2)
as prepared	[Au] 18.3	substrate	Au(4f$_{7/2}$) 84.0	Au^0	$(4.0 \pm 0.5) \times 10^{15}$
	[Fe] 6.3	[Fe] 38.5	Fe(2p$_{3/2}$) 710.9	Fe^{3+}	
	[O] 17.6	[O] 61.5	O(1s) 529.9	Fe−O	
			O(1s) 531.5	−OH	
			O(1s) 533.1	water	
	[C] 57.6		C(1s) 285.0	hydrocarbons	
100 °C	[Au] 18.8	substrate	Au(4f$_{7/2}$) 83.9	Au^0	$(3.6 \pm 0.5) \times 10^{15}$
30 min	[Fe] 7.3	[Fe] 40.0	Fe(2p$_{3/2}$) 710.9	Fe^{3+}	
	[O] 18.2	[O] 60.0	O(1s) 529.9	Fe−O	
			O(1s) 532.6	−OH + water	
	[C] 55.6		C(1s) 284.7	hydrocarbons	
further	[Au] 15.5	substrate	Au(4f$_{7/2}$) 83.9	Au^0	
200 °C	[Fe] 10.7	[Fe] 40.0	Fe(2p$_{3/2}$) 710.9	Fe^{3+}	
30 min	[O] 21.1	[O] 60.0	O(1s) 529.9	Fe−O	
			O(1s) 532.1	−OH	
	[C] 52.7		C(1s) 284.7	hydrocarbons	
further	[Au] 15.2	substrate	Au(4f$_{7/2}$) 84.0	Au^0	
300 °C	[Fe] 14.2	[Fe] 39.0	Fe(2p$_{3/2}$) 710.7	Fe^{3+} (+Fe^{2+})	
30 min	[O] 23.0	[O] 61.0	O(1s) 530.0	Fe−O	
			O(1s) 532.7	−OH	
	[C] 47.6		C(1s) 284.7	hydrocarbons	
further	[Au] 12.7	substrate	Au(4f$_{7/2}$) 84.0	Au^0	
400 °C	[Fe] 16.6	[Fe] 45.0	Fe(2p$_{3/2}$) 710.6	Fe^{3+}(+Fe^{2+})	
30 min	[O] 22.2	[O] 55.0	O(1s) 530.1	Fe−O	
			O(1s) 532.1	−OH	
	[C] 48.5		C(1s) 284.9	hydrocarbons	
further	[Au] 10.4	substrate	Au(4f$_{7/2}$) 84.3	Au^0	
600 °C	[Fe] 23.0	[Fe] 45.0	Fe(2p$_{3/2}$) 710.1	Fe^{2+}	
30 min			Fe(2p$_{3/2}$) 706.9	Fe^0	
	[O] 22.0	[O] 55.0	O(1s) 530.3	Fe−O	
	[C] 44.6		C(1s) 284.5	graphite	

[a] Determined as if the sample were homogeneous mixture of its constituents. [b] See text for details.

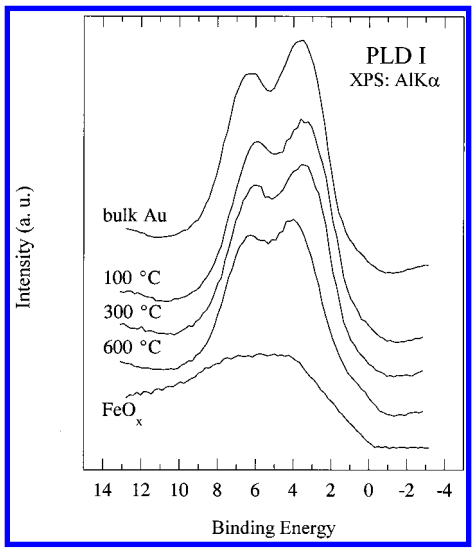

Figure 6. XPS valence band spectra of PLD I heat-treated in a vacuum at the indicated temperatures.

gives an increasing contribution to the photoemission intensity observable at the Fermi level. Moreover, a gradual decrease of the amount of the gold was observed.

To explain these facts we suggest that partially reduced iron oxide species migrate to the surface and partially cover the gold particles. This migration could be another possible explanation for the decreasing surface Au content. The small shift in the Au 4f binding energy as well as the lower binding energy of the Au 5d states, accompanied by the narrowing valence bandwidth, unambiguously shows changes in the local environment of the gold in accordance with the appearance of an iron oxide layer on the top of Au. Nevertheless, the described structural change of the sample led to the diminished catalytic activity in CO oxidation (see later), although the sample still contains significant amounts of gold.

TABLE 4: Core Level Characteristics of in Situ Pretreated PLD I and PLD II Samples

treatment	PLD I obsd peaks	PLD I BE (eV)	PLD I amount of Au/mg	PLD II obsd peaks	PLD II BE (eV)	PLD II amount of Au/mg
as prepared	Au(4f)	84.2	7.88×10^{-4}	Au(4f)	84.3	15.23×10^{-4}
	Fe(2p)	710.7		Fe(2p)	710.8	
oxidized	Au(4f)	84.5	6.30×10^{-4}	Au(4f)	84.5	6.34×10^{-4}
	Fe(2p)	711.3		Fe(2p)	711.3	
reduced	Au(4f)	84.5	5.25×10^{-4}	Au(4f)	84.6	2.53×10^{-4}
	Fe(2p)	710.4		Fe(2p)	710.7	

3.2.2. In Situ XPS and TEM Studies on Oxidation and Reduction of the Samples. After oxidation of the PLD I and PLD II samples the XPS spectra show very similar states for both FeO_x and Au particles as shown in Table 4. Both samples have similar Au loading with regard to a few atomic layers at the outer surface of the samples and this is important for the catalytic reaction. After oxidation and reduction the Au 4f peaks did not show any appreciable shift being at 84.5 eV. After reductive treatment in hydrogen the decrease in the gold content is apparent.

In the as-prepared state Fe 2p has a BE value of 710.7−710.8 eV which is assigned to Fe^{3+} state in the form of Fe_2O_3 or FeO(OH) as also shown in Table 4. However, significant shifts of about 1 eV can be observed for the Fe 2p peaks in both types of samples according to oxidation and reduction. The unchanged position of the Au peaks in the XPS spectra after oxidation and reduction pretreatments is likely ascribed to the presence of FeO_x stabilizing the gold electronic levels, along with the decreasing surface gold concentration detected. The Fe 2p binding energy values change in the expected direction during pretreatments: annealing in a vacuum and hydrogen

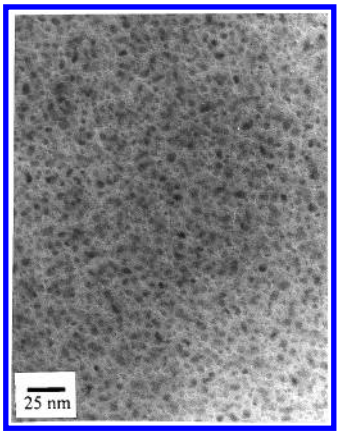

Figure 7. Plan-view TEM micrograph of the as-prepared PLD I sample.

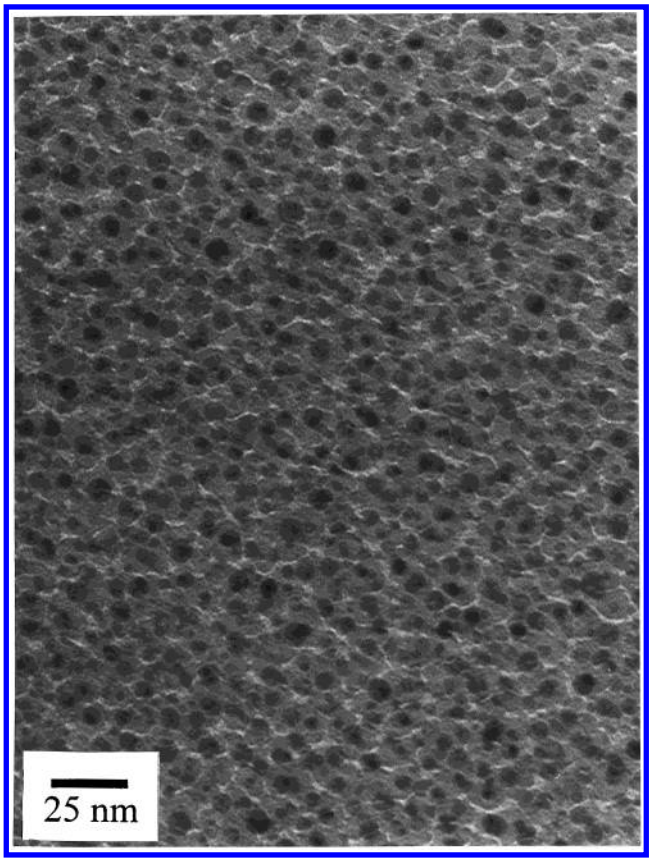

Figure 8. Plan-view TEM micrograph of the oxidized PLD I sample.

somewhat reduces the iron oxides, while heat treatment in oxygen increases the level of oxidation.

In the following we discuss TEM results obtained on the oxidized and reduced PLD I sample. The same pretreatment was applied as during catalytic reactions. Figures 7−9 show plan-view TEM micrographs of the gold islands on FeO_x supported by carbon-coated TEM microgrids. The most remarkable change induced by these treatments is visible in the FeO_x support material, similarly to what was observed in the PLD II samples. While in the as-prepared state (Figure 7) the support material gives only a weak contrast, it becomes darker during the treatments. Moreover, in the electron diffraction pattern of the as-prepared and oxidized sample only the rings of polycrystalline Au can be identified. After reduction, however, two weak rings due to a new crystalline FeO_x phase become observable. This phase can be identified as maghemite-c, which is the cubic form of the Fe_2O_3 compared to the rhombohedral form of the Fe_2O_3 hematite. The size distribution of the islands from the micrographs given on Figures 10−12 shows continuous evolution from a highly asymmetric distribution with many small particles toward a much more symmetric ones accompanied by an increase of the average size. It is important to emphasize that in the as-prepared sample the FeO_x support gives a more or less amorphous contrast with several dark spots in a relatively broad size range. These objects are identified as gold islands of 3.8 nm average diameter size. In the electron diffraction pattern, rings of polycrystalline gold particles are clearly present. Presence of some crystalline FeO_x phase cannot be completely ruled out as their rings (especially for Fe_2O_3) overlap with those of Au. Concerning the oxidative and reductive treatments, we can establish that after oxidation the size of Au particles slightly increases (4.1 nm) and the size distribution of the amorphous FeO_x becomes more homogeneous. In the electron diffraction pattern only the Au bands can be seen in both cases. In the reduced sample the diameter of gold further increases (5 nm) and two new FeO_x lines in the electron diffraction picture are developed.

As a short summary of the electron spectroscopic and TEM results, a close similarity between the PLD I and PLD II systems is established. The pulsed laser deposited support material forms an amorphous structure, regardless of its actual composition. During treatments applied in a catalytic process it transforms into a more dense, at least partially crystalline and somewhat reduced phase. During this transformation the gold content of the regions close to the surface significantly decreases. Finally, in the PLD II sample gold seems to be somewhat more dispersed than in PLD I catalysts.

3.3. Catalytic Results. The initial rates of CO oxidation were determined on the samples treated in different ways. In the preliminary experiments, the amount of CO_2 (n_{CO_2}) in the gas mixture referring to 1 mg of catalyst was measured from the intensity data of the mass spectrometer to obtain comparable data with that obtained with samples that contain no Au. In the reaction of the PLD I and PLD II samples the amount of CO_2 formed was measured relative to 1 mg of Au. The initial reaction rate (r_0) was evaluated using the plots of n_{CO_2}−time data. From the equation of the fitted curves r_0 was determined as the slope of the kinetic curve extrapolated to zero time. The reactivity of the samples investigated in the preliminary experiments decreases in the sequence $Au/FeO_x/SiO_x/Si(100) > FeO_x/SiO_x/Si(100) > Au/SiO_x/Si(100) > Si(100)$.

The $Au/FeO_x/SiO_x/Si(100)$ catalyst has the highest initial activity. The results along with XPS and TEM data demonstrate that the interaction of gold nanoparticles and iron oxide tends to stabilize the metal character of gold and due to this stabilization, the Au/FeO_x catalyst has enhanced activity in the CO oxidation.

Conflicting data are available in the literature on how the structure of the gold catalysts is changed with various treatments. Calcination of the Au/TiO_2 sample with increasing temperature in air or in hydrogen increased or decreased the particle size, respectively.[39] Accordingly, the activity in CO oxidation was increased with the calcination temperature which was interpreted by the authors with the reduction of $Au(OH)_3$ and the formation of a Au/TiO_2 perimeter interface. In contrast to this study, an increase of the calcination temperature decreased the activity in CO oxidation for the Au/Fe_2O_3 catalyst, which was explained by the valence state change of gold from $Au(OH)_3$ via Au_2O_3 to metallic gold as proved by XPS studies.[40] The scenario became even more complicated when Au/TiO_2 and Au/ZrO_2 samples were compared.[41] In the latter case, activity in CO

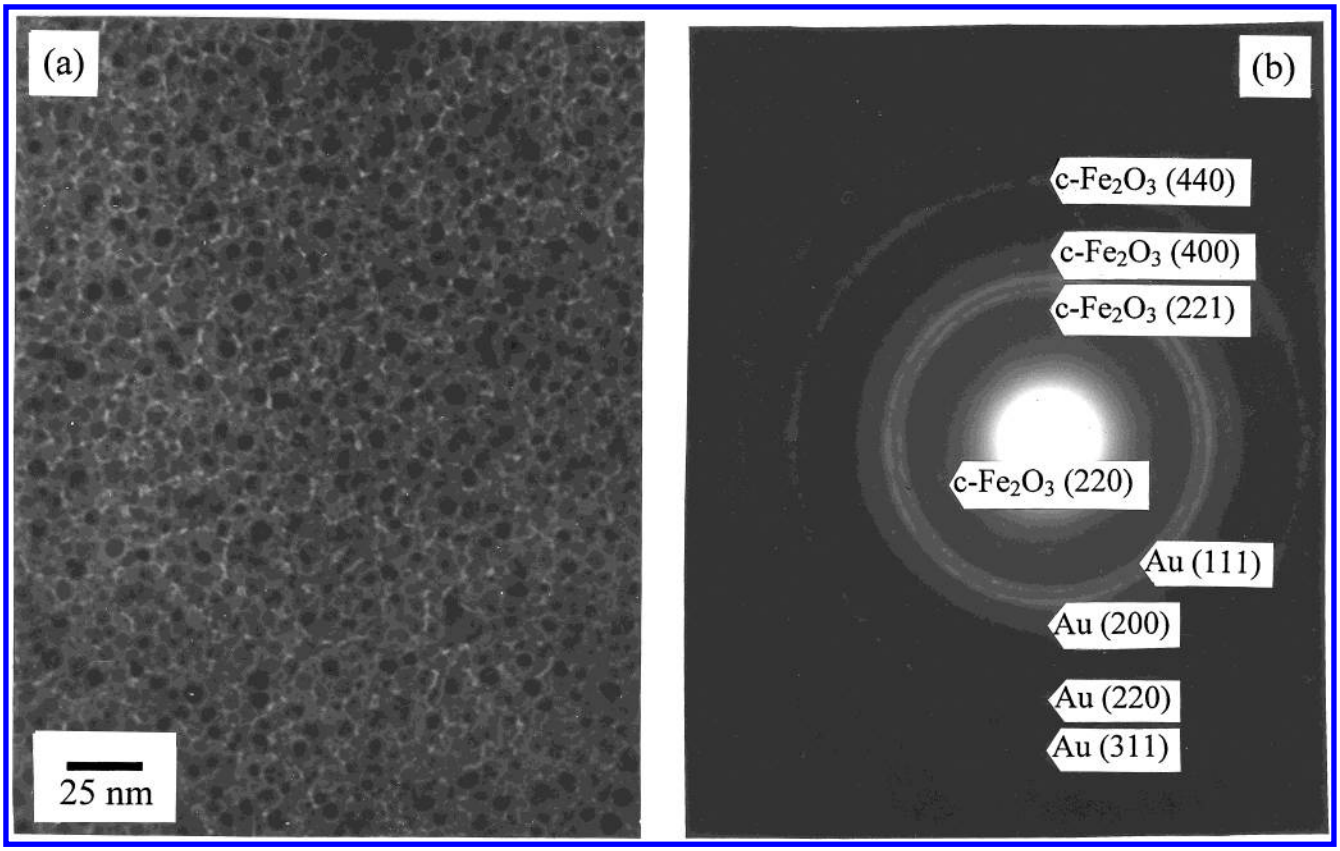

Figure 9. (a) Plan-view TEM micrograph of the reduced PLD I sample; (b) electron diffraction pattern for the reduced PLD I sample.

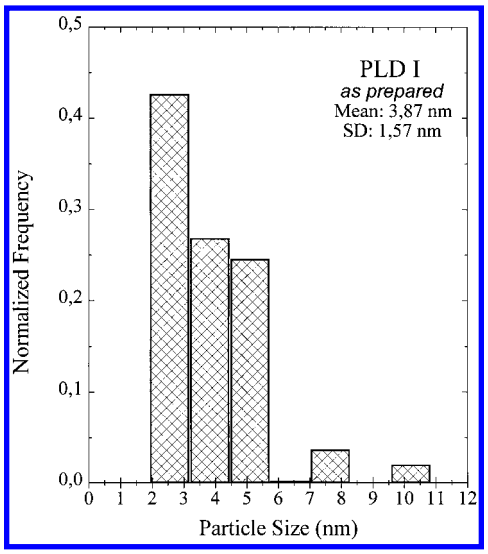

Figure 10. Size distribution of the as-prepared PLD I sample.

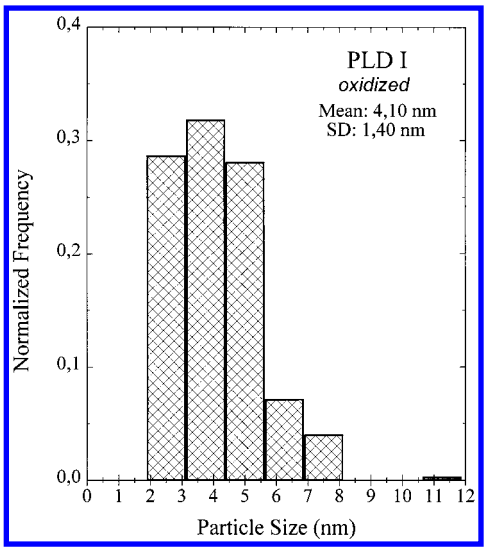

Figure 11. Size distribution of the oxidized PLD I sample.

oxidation was observed only after calcination. In the latter case, positively polarized gold atoms were suggested to be responsible for the CO oxidation activity.

Single-crystal studies,[42] however, indicated that when metallic gold is evaporated on a single crystal of TiO_2 (and not starting from Au ions), the maximum in catalytic activity starts when the electron structure of gold is just at the border of the transition between ionic (large band gap) and metallic character. That is, for the catalytic activity metallic gold is required, but, beyond this, a strong interaction between the metal and support along the perimeter interface.

Bearing this in mind, we are now in the position to try to interpret the correlation between XPS andTEM data and catalytic experiments performed on PLD I and PLD II samples after different pretreatments. The two types catalysts show very similar behavior after the same pretreatments. In both cases the oxidized samples show the best activity in the CO oxidation reaction. There are two reasons: (i) first, on oxidation the contaminating layer can be removed and (ii) amorphous highly oxidized iron oxide can be stabilized. However, reduction by H_2 leads to significant decrease in activity in both cases partly due to the reduction of iron (XPS data) and formation of a partially crystalline structure (TEM). Nevertheless, the PLD II sample shows a smaller decrease in activity. This is in good agreement with the result of the XPS measurements; i.e., this sample remains in a more oxidized state after reduction relative to the PLD I sample. In Table 5 the results of catalytic activity of the samples are presented.

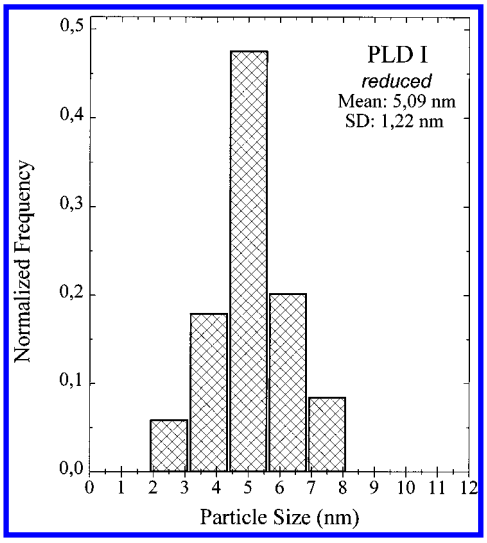

Figure 12. Size distribution of the reduced PLD I sample.

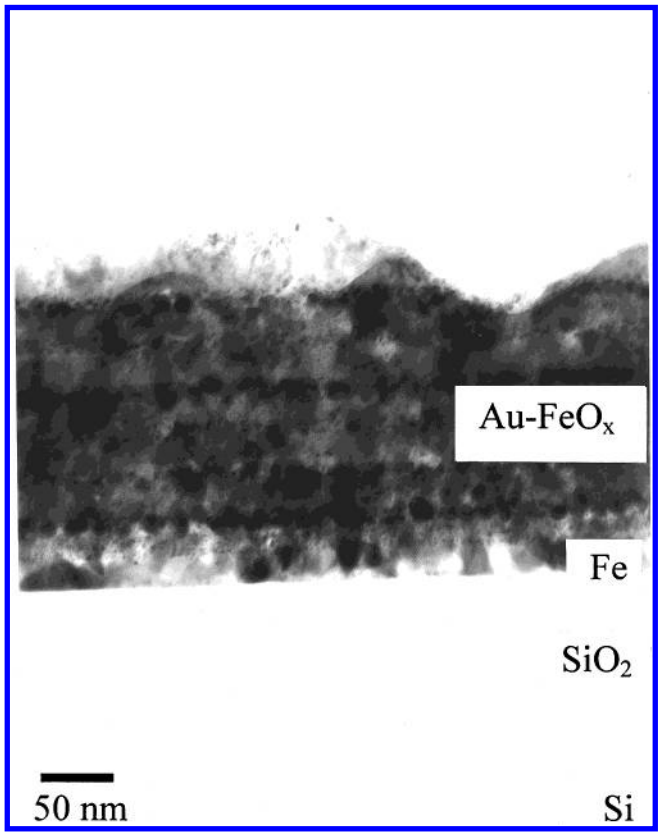

Figure 13. Cross-sectional TEM micrograph of the PLD II sample after catalytic measurements.

TABLE 5: Catalytic Activity of the PLD I and PLD II Samples Measured as 250 °C

treatment	activity of PLD I (μmol CO_2/(mg_{Au} min))	activity of PLD II (μmol CO_2/(mg_{Au} min))
as prepared	13.71	2.08
oxidized	35.24	34.18
reduced	2.15	10.05

During catalytic measurements, especially after reduction, the sample lost its catalytic activity. This behavior is accompanied by dramatic structural changes, as can be seen in the PLD II sample in Figure 13. The originally flat surface became rough, showing hills and valleys in the 50−100 nm size range. The protuberances seem to have grown on the top of the original sample surface and the regions of gold particles are still clearly visible. In addition, the originally amorphous microstructure transformed into a more compact one. Dark field images (not shown) reveal that the protuberances are crystalline. Similarly to the electron diffraction pattern of the reduced PLD I sample (Figure 9b) the presence of maghemite-c can be identified.

The third reason for the diminished activity of the reduced samples is the disappearance of gold from the surface. Electron spectroscopic investigations proved that the gold content at the surface of both types of reduced catalyst is almost $1^1/_2$ orders of magnitude lower than that of the freshly prepared sample (Table 6). The weak Au 4f peaks of the PLD II sample are somewhat shifted toward lower binding energies, showing a different local environment compared to the as-prepared state. This also indicates an increase in the gold particle size as was shown in Figure 12. The sample is covered by a relatively thick contamination layer, which can be successfully removed by ion bombardment. Under this overlayer, iron seems to be slightly more reduced when compared to the freshly prepared catalyst.

The distribution of the gold in depth in the used PLD II sample was determined by XPS depth profiling using 2 keV Ar^+ ions. The concentration of gold gradually increased, as the protuberances were etched away, and finally reached a value which is somewhat smaller than, but comparable to that of, the freshly prepared catalyst (see Table 6). The binding energy of the Au 4f peaks became the same as observed before catalytic measurements. On the other hand, the iron in the FeO_x matrix was clearly reduced, and a small component in the Fe 2p spectrum due to Fe^0 appeared, while the main component was identified as Fe^{2+}. This effect may perhaps be due to the reductive effect of sputtering, but it cannot be ruled out that during catalytic treatment the whole FeO_x matrix suffered a partial reduction.

We have also investigated the PLD I sample after completing the catalytic cycle. Again, in close agreement with the observations obtained on the PLD II after catalytic measurement, the gold was not detectable at the surface of the catalyst (see Table 7). Subsequent oxidation after the catalytic reaction resulted in restoring the activity in both cases.

To sum up, it can be established that for developing significant catalytic activity we need (i) the presence of metallic gold particles (3−4 nm in diameter), (ii) amorphous iron oxide support in oxidized state with significant interfacing with gold particles along the perimeter, and (iii) slightly reduced iron oxide as support with oxygen defect sites.

The presence of these three factors may create the sites along the gold/support perimeter which are a prerequisite for high catalytic activity in CO oxidation.

Indeed, in the most active samples the Fe 2p lines show the same oxidation states in the XPS spectra which could be a mixture of iron hydroxide and Fe_2O_3. TEM photographs from oxidized PLD I show an amorphous FeO_x layer. Both types of reduced samples have similar positions of the Fe peaks in the XPS spectra, which could be assigned to Fe_2O_3 or FeO diffraction patterns of both reduced catalysts. New lines due to maghemite-c crystallites (cubic form of Fe_2O_3) also appeared. Reductive treatment clearly leads to decrease of the catalytic activity which is due to the transition from the amorphous to a partially crystalline phase and reduction of iron.

The lack of catalytic activity of the PLD I sample after annealing in a vacuum up to 600 °C can clearly be ascribed to the fact that a strong interaction is not present anymore. The annealing also caused the reduction of the Fe particles and decreased the gold content of the surface, which led to the least reactive form of the catalyst, as also obtained by H_2 reduction.

TABLE 6. Composition and Core Level Characteristics of PLD II Sample after Catalytic Reaction[a]

treatment	composition (atom %)[b] as measured	composition (atom %)[b] corrected[c]	binding energy (eV)	chemical state	Au density (atoms/cm^3)
	[Au] 0.05	[Au] 0.2	Au($4f_{7/2}$) 83.7		
as prepared	[Fe] 7.0	[Fe] 46.3	Fe($2p_{3/2}$) 710.7	$Fe^{3+} + Fe^{2+}$	
(after reduction)	[O] 19.5	[O] 53.5	O(1s) 529.8	Fe−O	
			O(1s) 531.9	−OH	
	[C] 73.4	$D_C \approx 2.1$ nm	C(1s) 284.9	hydrocarbons	
2 min 2 keV	[Au] 0.2	[Au] 0.2	Au($4f_{7/2}$) 83.8		$(2.0 \pm 1.0) \times 10^{20}$
Ar^+ ion	[Fe] 28.7	[Fe] 47.8	Fe($2p_{3/2}$) 710.2	mostly Fe^{2+}	
bombardment	[O] 34.3	[O] 52.0	O(1s) 529.9	Fe−O	
	[C] 36.9	$D_C \approx 0.7$ nm	C(1s) 284.8	hydrocarbons	
80 min 2 keV	[Au] 1.8		Au($4f_{7/2}$) 84.3		$(2.0 \pm 1.0) \times 10^{21}$
Ar^+ ion	[Fe] 50.5		Fe($2p_{3/2}$) 709.9	Fe^{2+}	
bombardment			Fe($2p_{3/2}$) 707.2	Fe^0	
	[O] 36.4		O(1s) 530.1	Fe−O	
	[C] 11.3		C(1s) 284.5	graphite	

[a] Catalytic measurement involves a complete activity measurement−xidation−activity measurement−reduction−activity measurement cycle. [b] Determined as if Au would be homogeneously dispersed throughout the FeO matrix. [c] Corrected for carbon- and oxygen-containing overlayer as described in ref 36.

TABLE 7: Composition and Core Level Characteristics of the PLD II Sample after catalytic reaction[a]

treatment	composition (atom %) as measured[b]	composition (atom %) corrected[c]	binding energy (eV)	chemical state	surface Au (atoms/cm^2)
	[Au] 0.0	[Au] 0.0	Au($4f_{7/2}$)		not detectable
as prepared	[Fe] 24.8	[Fe] 42.8	Fe($2p_{3/2}$) 711.0	Fe^{3+} (+Fe^{2+})	
(after reduction)	[O] 41.9	[O] 57.2	O(1s) 529.9	Fe−O	
			O(1s) 531.7	−OH	
			O(1s) 533.0	water	
	[C] 33.4	$D_c \approx 0.7$ nm	C(1s) 285.0	hydrocarbon	
	[Au] 0.0	[Au] 0.0	Au($4f_{7/2}$)		
1 min 2 keV	[Fe] 34.4	[Fe] 47.7	Fe($2p_{3/2}$) 710.5	$Fe^{3+} + Fe^{2+}$	not detectable
Ar^+ ion	[O] 43.5	[O] 52.3	O(1s) 529.8	Fe−O	
bombardmentt			O(1s) 531.6	−OH	
			O(1s) 533.3	water	
	[C] 22.1		C(1s) 284.6	hydrocarbon	

[a] Catalytic measurement involves a complete activity measurement−oxidation−activity measurement−reduction−activity measurement cycle. [b] Determined as if the sample were homogeneous mixture of its constituents. [c] Corrected for carbon- and oxygen-containing overlayer as described in ref 36.

4. Conclusions

(i) It was established that in a $Au/FeO_x/SiO_2/Si(100)$ model system the gold maintains its valence state even during size reduction. This is valid for the different treatments. However, the morphology of iron oxide layer and the valence state of iron in it depends on the various treatments.

(ii) TEM investigations revealed that in the PLD I sample in the as-prepared and oxidized samples the same amorpous iron oxide layer exits, but the valence state of iron varies. XPS measurements revealed the importance of the Fe^{3+} state in the oxidation reaction of CO. The size of gold particles does not change significantly. Because of this finding the oxidized sample has the best activity toward CO oxidation. The difference between PLD I and PLD II samples lies in the catalytic activity and in the higher crystallinity in the iron oxide layer for PLD II.

(iii) During reductive treatment (heating in a vacuum or in hydrogen) slight migration of both the support and the gold particles can be observed which resulted in a decrease of gold concentration at the outer surface. Furthermore, during reductive treatment the amorphous iron oxide was slightly crystallized and reduced into Fe^{2+} or Fe^0 species.

Acknowledgment. The authors gratefully acknowledge the financial support from the Research Fund of the Hungarian Academy of Sciences and the Hungarian Science and Research Fund (grant F 025890).

References and Notes

(1) Hagen, D. I.; Somorjai, G. A. *J. Catal.* **1976**, *41*, 466.
(2) Sachtler, J. W. A.; van Hove, M. A.; Biberian, J. P.; Somorjai, G. A. *Phys. Rev. Lett.* **1980**, *45*, 1601.
(3) Turkevich, J.; Kim, G. *Science* **1970**, *169*, 873.
(4) Cha, D. Y.; Parravano, G. *J. Catal.* **1970**, *18*, 200.
(5) Parravano, G. *J. Catal.* **1970**, *18*, 320.
(6) Schwank, J.; Galvagno, S.; Parravano, G. *J. Catal*. **1980**, *63*, 415.
(7) Galvagno, S.; Parravano, G. *J. Catal*. **1978**, *55*, 178.
(8) Bailar, J. C. *Comprehensive Inorganic Chemistry*; Pergamon Press: New York, 1973.
(9) Puddephatt, R. J. *The periodic table of the elements*; Oxford University Press: London, 1972.
(10) Haruta, M.; Yamada, N.; Kobayashi, T.; Iijima, S. *J. Catal*. **1989**, *115*, 301.
(11) Haruta, M. *Catal. Today* **1997**, *36*, 153.
(12) Ueda, A.; Oshima, T.; Haruta, M. *Appl. Catal. B.* **1997**, *12*, 81.
(13) Andreeva, D.; Tabakova, T.; Idakiev, V.; Christov, P.; Giovanoli, R. *Appl. Catal. A.* **1998**, *169*, 9.
(14) Sakurai, H.; Haruta, M. *Catal. Today* **1996**, *29*, 361.
(15) Haruta, M.; Ueda, A.; Tsubota, S.; Torres Sanches, R. M. *Catal. Today* **1996**, *29*, 443.
(16) Yuan, Y.; Asakura, K.; Wan, H.; Tsai, K.; Iwasawa, Y. *Chem. Lett.* **1996**, 755.
(17) Kozlova, P.; Kozlov, I.; Sugiyama, S.; Matsui, Y.; Asakura, K.; Iwasawa, Y. *J. Catal.* **1999**, *181*, 37.
(18) Wagner, F. E.; Galvagno, S.; Milone, C.; Visco, A. M. *J. Chem. Soc., Faraday Trans.* **1997**, *93*, 3403.
(19) Minico, S.; Sciere, S.; Crisafulli, C.; Visco, A. M.; Galvagno, S. *Catal. Lett.* **1997**, *47*, 273.
(20) *Proceedings of the 8th International Symposium on Heterogeneous Catalysis*; Andreev, A., Petrov, L., Bonev, Ch., Kadinov, G., Mitov, I., Eds.; Varna, 1996; p 141.

(21) Guillemot, D.; Polisset-Thofin, M.; Bonnin, D.; Borovkov, V. Yu.; Fraissard, J. In *Proceedings of the 12th International Zeolite Conference*; Treacy, M. M., Marcus, B. K., Bisher, M. E., Higgins, J. B., Eds.; Materials Research Society: Warrendale, 1999; Vol 4, p 2809.

(22) Guillemot, D.; Polisset-Thofin, M.; Fraissard, J. *Catal. Lett*. **1996**, *41*, 143.

(23) Guillemot, D.; Borovkov, V. Yu.; Kazansky, V. B.; Polisset-Thofin, M.; Fraissard, J. *J. Chem. Soc., Faraday Trans.* **1997**, *93*, 3587.

(24) Salama, T. M.; Ohnishi, R.; Shido, T.; Ichikawa, M. *J. Catal*. **1996**, *162*, 169.

(25) Berko, A.; Klivényi, G.; Solymosi, F. *J. Catal*. **1999**, *182*, 511.

(26) Cunningham, D. A.; Vogel, W.; Kageyama, H.; Tsubota, S.; Haruta, M. *J. Catal*. **1998**, *177*, 1.

(27) Haruta, M. *Catal. Surveys Jpn*. **1997**, *1*, 61.

(28) Eppler, A. S.; Rupprechter, G.; Guczi, L.; Somorjai, G. A. *J. Phys. Chem. B* **1997**, *101*, 9973.

(29) Serna, R.; Missana, T.; Afonso, C. N.; Ballesteros, J. M.; Petford-Long, A. K.; Doole, R. C. *Appl. Phys. A* **1998**, *66*, 43.

(30) Pászti, Z.; Horváth, Z. E.; Petõ, G.; Karacs, A.; Guczi, L. *Appl. Surf. Sci*. **1997**, *109/110*, 67.

(31) Boldyreva, N. A.; Yatsimirsky, V. K. In *Proceedings of the 10th International Congress on Catalysis*; Guczi, L., Solymosi, F., Tétényi, P., Eds.; Akadémiai Kiadó, Budapest, 1993; Vol. 3, p 2621.

(32) Upchurch, B. T.; Kielin, E. J.; Schryer, D. E. *Catal. Lett*. **1995**, *31*, 153.

(33) Haruta, M.; Tsubota, S.; Kobayashi, T.; Kageyama, H.; Genet, M. J.; Delmon, B. *J. Catal*. **1993**, *144*, 175.

(34) Lin, S. D.; Bollinger, M.; Vannice, M. A. *Catal. Lett*. **1993**, *17*, 245.

(35) Haruta, M.; Kobayashi, T.; Sano, H.; Yamada, N. *Chem. Lett*. **1987**, 405.

(36) Zalm, P. C. *Surf. Interface Anal*. **1998**, *26*, 352.

(37) Kennedy, R. J. *IEEE Trans. Magn.* **1995**, *31*, 3829.

(38) Kleint, C. A.; Semmelhack, H. C.; Lorenz, M.; Krause, M. K. *J. Magn. Magn. Mater*. **1995**, *140*−*44*, 725.

(39) Tsubota, S.; Cunnigham, D. A. H.; Bando, Y.; Haruta, M. In *Preparation of Catalysts VI*; Poncelet, G., Martens, J., Delmon, B., Jacobs, P. A., Grange, P., Eds.; Stud. Surf. Sci. Catal.; Elsevier Science: Amsterdam, 1994; Vol. 91, p 22.

(40) Park, E. D.; Lee, J. S. *J. Catal*. **1999**, *186*, 1.

(41) Grunwaldt, J.-D.; Maciejewski, M.; Becker, O. S.; Fabrizioli, P.; Baiker, A. *J. Catal*. **1999**, *186*, 458.

(42) Valden, M.; Lai, X.; Goodman, D. W. *Science* **1998**, *281*, 1647.